Transferred hyperfine interaction at 295 K between the rare-earth ions and the fluorine and lithium nuclei in lithium rare-earth fluorides *

P. E. Hansen and R. Nevald
Department of Electrophysics, The Technical University of Denmark, DK-2800 Lyngby, Denmark
(Received 2 March 1976; revised manuscript received 9 August 1976)

The nuclear-magnetic-resonance rotation spectra for the fluorine and lithium nuclei in $LiTbF_4$, $LiDyF_4$, $LiHoF_4$, and $LiErF_4$ have been obtained at 295 K. They are separated in contributions from the dipole and the transferred hyperfine interactions. In general, the latter consists of an isotropic part and an anisotropic part. The anisotropic part turns out to be very small in all cases when the uniaxial anisotropy of the susceptibility of the crystal has been accounted for. Both for fluorine and lithium the isotropic transferred hyperfine interaction is found to make the local field lower than the applied field. The results are discussed in view of current theories.

I. INTRODUCTION

The tetragonal scheelite-type crystals $LiR_xY_{1-x}F_4$ (where R is a rare-earth ion) are attracting much attention due to their efficient laser action, and their relative structural simplicity. Furthermore, the dense crystals exhibit (dominantly) dipole-coupled ordered phases at low temperature.

In this laboratory we have undertaken a many aspect study of these interesting materials. In recent works we (Hansen *et al.*[1,2]) determined the static magnetic behavior, and the crystal-field parameters at the R and Li sites in the dense crystals $LiTbF_4$, $LiDyF_4$, $LiHoF_4$, and $LiErF_4$. Here we report on the transferred hyperfine interactions between the R and the F and Li nuclei, and in a subsequent paper we want to discuss the dynamical aspects of the magnetic behavior.

The transferred hyperfine interactions, presented here, have been deduced from the NMR rotation spectra of the ^{19}F and ^{7}Li nuclei. Similar work has been performed in numerous compounds with $3d$-group magnetic ions. The data collected so far about the interaction between ^{19}F and rare-earth ions are much fewer. Most work[3-19] has been done using ESR and electron-nuclear double-resonance techniques at low temperatures and the interest has concentrated on the materials CaF_2, BaF_2, SrF_2, and CdF_2 of fluorite structure doped with various rare-earth ions, which enter sites with cubic, tetragonal, and trigonal symmetry. Low-temperature NMR has been done in one case[20] and several results[21-24] at high temperature have been reported. The interpretation of systems doped with R ions is somewhat complicated by the lack of knowledge of the exact bond length between the fluor and rare-earth ions. In the $LiRF_4$ the positions of the ions are known and together with the approximate known eigenfunctions this system should provide a good basis for theoretical calculations.

II. THEORY

The unit cell of the scheelite structure ($I4_1/a$) consists of four formula units, a, b, c, and d (Fig. 1). Because the structure is body centered,

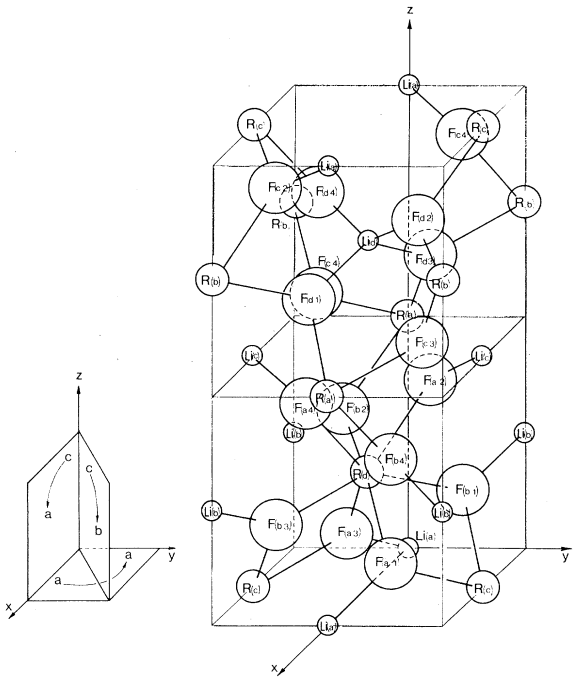

FIG. 1. Crystal structure of $LiRF_4$. One unit cell is shown, which contains four formula units. The ions a and b are connected to the ions c and d through the $(\frac{1}{2},\frac{1}{2},\frac{1}{2})$ translations. The ions a and c are connected to the ions b and d through the inversion centers. The F_1, F_2, F_3, and F_4 are related by the $\bar{4}$ axes. The inset shows the three planes of H-field rotation applied in the experiments.

the ions of c and d are in physical equivalent positions to the ions of a and b. Furthermore the ions of b are connected to the ions of a through the inversion center, which means that their behavior with respect to a magnetic field of any orientation will be identical. Therefore only the positions of the ions in one formula unit need to be considered in details: The four F's are in general positions (x, y, z), $(\bar{y}, x, \bar{z})$, $(\bar{x}, \bar{y}, z)$, and $(y, \bar{x}, \bar{z})$ connected by the $\bar{4}$ axis. The Li and R are situated on the $\bar{4}$ axis in the $(0, 0, 0)$ and $(0, 0, \frac{1}{2})$ positions, respectively.

If a magnetic field $\vec{H}_a$ is applied to a spherical sample, the inner macroscopic magnetic field $\vec{H}_i$ is given by

$$\vec{H}_i = \vec{H}_a - \tfrac{4}{3}\pi\vec{M} = \vec{H}_a - \tfrac{4}{3}\pi\rho\vec{\chi}\cdot\vec{H}_i$$

or

$$(1 + \tfrac{4}{3}\pi\rho\vec{\chi})\cdot\vec{H}_i = \vec{H}_a , \tag{1}$$

where the mass susceptibility $\vec{\chi}$ is diagonal in the crystalline system of axes with $\chi_{aa} = \chi_{bb} = \chi_\perp$ and $\chi_{cc} = \chi_\parallel$.

The local magnetic field $\vec{H}_n^j$ at the jth nucleus of type n (Li or F) may, for a spherical sample, be written

$$\vec{H}_n^j = \vec{H}_a + [(\zeta_n\vec{1} + \vec{\alpha}_n^j)/\rho]\cdot\vec{M} = \vec{H}_a + (\zeta_n\vec{1} + \vec{\alpha}_n^j)\cdot\vec{\chi}\cdot\vec{H}_i , \tag{2}$$

where $\vec{\alpha}_n^j$ is the traceless part of the mean-field tensor $\vec{\alpha}_n^j = \vec{\delta}_n^j + \vec{\epsilon}_n^j$. $\vec{\delta}_n^j\cdot\vec{M}/\rho$ is the magnetic dipole contribution to the local field, given by

$$\vec{\delta}_n^j = \kappa \sum_{\substack{k \text{ in a} \\ \text{sphere}}} \frac{3\vec{r}_{nk}^j\vec{r}_{nk}^j - \vec{1}(r_{nk}^j)^2}{(r_{nk}^j)^5} , \tag{3}$$

κ being the mass per formula unit and $\vec{r}_{nk}^j$ the vector from the jth ion of type n to the kth R neighbor. $\zeta_n\vec{1} + \vec{\epsilon}_n^j$ takes into account — in the mean-field approximation — isotropic and anisotropic transferred hyperfine interaction, abbreviated ITH and ATH, respectively.

From (1) and (2) one gets

$$\vec{H}_n^j = \vec{H}_a + (\zeta_n\vec{1} + \vec{\alpha}_n^j)\cdot\vec{\chi}\cdot(\vec{1} + \tfrac{4}{3}\pi\rho\vec{\chi})^{-1}\cdot\vec{H}_a = [\vec{1} + (\zeta_n\vec{1} + \vec{\alpha}_n^j)\cdot\vec{\chi}\cdot(\vec{1} + \tfrac{4}{3}\pi\rho\vec{\chi})^{-1}]\cdot\vec{H}_a . \tag{4}$$

In this work all data are taken at 295 K, at which temperature $\frac{4}{3}\pi\rho\chi_{ii} < 0.5\%$ for any i and all compounds investigated. (See Table I.) Therefore $\vec{H}_n^j$ is approximately

$$\vec{H}_n^j = [\vec{1} + (\zeta_n\vec{1} + \vec{\alpha}_n^j)\cdot\vec{\chi}]\cdot\vec{H}_a . \tag{5}$$

$\vec{\alpha}_{\mathrm{Li}}$ (and $\vec{\alpha}_R$) are diagonal and $\alpha_{\mathrm{Li}\,xx} = \alpha_{\mathrm{Li}\,yy}$, because of the position on the $\bar{4}$ axis. $\vec{\alpha}_{\mathrm{F}}^j$ is nondiagonal, but the following symmetry connections exist:

$$\alpha_{\mathrm{F}\,xx}^{j+1} = \alpha_{\mathrm{F}\,yy}^{j}, \quad \alpha_{\mathrm{F}\,yy}^{j+1} = \alpha_{\mathrm{F}\,xx}^{j}, \quad \alpha_{\mathrm{F}\,zz}^{j+1} = \alpha_{\mathrm{F}\,zz}^{j},$$
$$\alpha_{\mathrm{F}\,xy}^{j+1} = -\alpha_{\mathrm{F}\,xy}^{j}, \quad \alpha_{\mathrm{F}\,xz}^{j+1} = \alpha_{\mathrm{F}\,yz}^{j}, \quad \alpha_{\mathrm{F}\,yz}^{j+1} = -\alpha_{\mathrm{F}\,xz}^{j},$$
$$j = 1, 2, 3 \tag{6}$$

(The F Nos. 2, 3, and 4 are reached from F No. 1 by application of the $\bar{4}$ symmetry 1, 2, and 3 times. See Fig. 1.)

In NMR the relative shift Δ in the magnitude of the magnetic field at the nucleus is measured, which using (5) approximately becomes

$$\Delta(v) = \Delta H_n^j/H_a = (H_n^j - H_a)/H_a = \vec{1}_H\cdot(\vec{1}\zeta_n + \vec{\alpha}_n^j)\cdot\vec{\chi}\cdot\vec{1}_H , \tag{7}$$

where $\vec{1}_H$ is a unit vector in the direction of H_a.

Experimentally Δ has been determined for H_a rotating in three planes: (i) In the crystal basal plane from one a axis to the next, 90 deg away ($a \rightarrow a$ rotation); (ii) From the c axis to the a axis ($c \rightarrow a$ rotation); (iii) From the c axis to the direction in the basal plane midway between two a axis ($c \rightarrow b$ rotation). The planes of rotation are indicated in Fig. 1. (The angle v is measured from

TABLE I. Material parameters used in this paper: (1) Lattice constants a and c; (2) volume of a unit cell (containing four formula units), V; (3) mass of one formula unit, κ; (4) mass density ρ; (5) Landé factor g_J; (6) mass susceptibilities $\chi_\perp$ and $\chi_\parallel$ at 295 K; (7) maximum field shift correction $\frac{4}{3}\pi\rho\chi_{\max}$, which is omitted.

Material	(1) a (Å)	(1) c (Å)	(2) V (Å^3)	(3) κ (10^{-22} g)	(4) ρ (g/cm^3)	(5) g_J	(6) $\chi_\perp$ (10^{-3} cm^3/g)	(6) $\chi_\parallel$ (10^{-3} cm^3/g)	(7) $\frac{4}{3}\pi\rho\chi_{\max}$ (%)
$LiTbF_4$	5.20	10.89	295	4.02	5.46	$\frac{3}{2}$	0.136	0.209	0.48
$LiDyF_4$	5.19	10.83	292	4.08	5.59	$\frac{4}{3}$	0.214	0.174	0.50
$LiHoF_4$	5.18	10.75	288	4.12	5.70	$\frac{5}{4}$	0.170	0.204	0.49
$LiErF_4$	5.16	10.70	285	4.15	5.83	$\frac{6}{5}$	0.156	0.134	0.38

the first mentioned crystalline direction to the direction of H_a.)

The angular dependence of the relative shifts is of the form

$$\Delta(v) = A_c \cos^2 v + A_s \sin^2 v + A_t \sin v \cos v . \quad (8)$$

The expressions for the "Fourier components" A_c, A_s, and A_t are obtained from (7) and given in Table II for the three rotations applied.

III. EXPERIMENTAL DETAILS

The single crystals were grown from 99.9% pure materials by the hydrofluorinating method described by Laursen and Holmes.[25] X-ray diffraction was used to confirm agreement with the structure and cell dimensions given by Keller and Schmutz,[26] as well as to select perfect samples. The samples of $LiTbF_4$, $LiHoF_4$, and $LiErF_4$ were grinded into spheres of approximately 3 mm in diameter. From $LiDyF_4$ only 1-mm faultless spheres could be obtained. In all cases the sphericality was better than 1%.

Each sphere was oriented directly in the NMR sample holder by conventional Laue x-ray technique. Except for $LiDyF_4$, a self-supporting five-turn coil of lacquered 0.5-mm-diam copper wire was placed around the sample and connected through a 0.5-m-long coaxial line to a Robinson-type NMR spectrometer. For the small $LiDyF_4$ sphere a 10-turn coil was molded in araldite from 0.15-mm-diam copper wire.

All spectra were obtained with the spectrometer frequency kept fixed, and the magnetic field was swept through the resonances and monitored with a field-locked NMR gaussmeter. The ^{7}Li and ^{19}F spectrum was recorded with the fixed spectrometer frequency in the range 11–14 MHz and 29–32 MHz, respectively.

For each crystal and for each type of resonating nuclei two series of spectra were taken. In one series the magnetic field was rotated $a \rightarrow a$, and in the other series either $c \rightarrow a$ or $c \rightarrow b$. The first combination applies to $LiDyF_4$ and $LiHoF_4$ and the second to $LiTbF_4$ and $LiErF_4$. In each series the magnetic field was rotated in steps between the individual recordings. A series consisted of at least seven recordings.

As an example the $LiDyF_4$ spectra for ^{19}F are shown in Fig. 2 and for ^{7}Li in Fig. 3. Also inserted in the figures are one of the actual recordings. (Although the volume of the $LiDyF_4$ sphere was 25 times smaller than the volume of the other spheres, the signal/noise did not appear smaller.)

In some ^{19}F spectra an unshifted resonance line was seen, which was traced to the lacquer of the copper coil. It served as an independent check on the value of applied magnetic field.

The figure shows immediately, that the number of lines for H_a in a general direction, and their

TABLE II. Fourier components of the relative field shift Δ at the F and Li sites for the three H_a-field rotations applied in the experiments.

Nucleus	Rotation	Fourier components of the local field shift $\Delta H/H$		
		$\cos^2 v$	$\sin^2 v$	$\sin v \cos v$
Li	$c \rightarrow a$, $c \rightarrow b$	$A_c = (\zeta - 2\alpha_{xx})\chi_{\parallel}$	$A_s = (\zeta + \alpha_{xx})\chi_{\perp}$	$A_t = 0$
(R)	$a \rightarrow a$	$B_c = (\zeta + \alpha_{xx})\chi_{\perp}$	$B_s = (\zeta + \alpha_{xx})\chi_{\perp}$	$B_t = 0$
F	$c \rightarrow a$, Dy, Ho, 1	$A_c = [\zeta - (\alpha_{xx} + \alpha_{yy})]\chi_{\parallel}$	$A_s^1 = (\zeta + \alpha_{xx})\chi_{\perp}$	$A_t^1 = \alpha_{xz}(\chi_{\parallel} + \chi_{\perp})$
	3			$A_t^3 = -A_t^1$
	2		$A_s^2 = (\zeta + \alpha_{yy})\chi_{\perp}$	$A_t^2 = \alpha_{yz}(\chi_{\parallel} + \chi_{\perp})$
	4			$A_t^4 = -A_t^2$
	$c \rightarrow b$, Tb, Er, 1	$A_c = [\zeta - (\alpha_{xx} + \alpha_{yy})]\chi_{\parallel}$	$A_s^1 = [\zeta + \alpha_{xy} + \frac{1}{2}(\alpha_{xx} + \alpha_{yy})]\chi_{\perp}$	$A_t^1 = [(\alpha_{xz} + \alpha_{yz})/\sqrt{2}](\chi_{\parallel} + \chi_{\perp})$
	3			$A_t^3 = -A_t^1$
	2		$A_s^2 = [\zeta - \alpha_{xy} + \frac{1}{2}(\alpha_{xx} + \alpha_{yy})]\chi_{\perp}$	$A_t^2 = -[(\alpha_{xz} - \alpha_{yz})/\sqrt{2}](\chi_{\parallel} + \chi_{\perp})$
	4			$A_t^4 = -A_t^3$
	$a \rightarrow a$, 1	$B_c^1 = (\zeta + \alpha_{xx})\chi_{\perp}$	$B_s^1 = (\zeta + \alpha_{yy})\chi_{\perp}$	$B_t^1 = 2\alpha_{xy}\chi_{\perp}$
	3			
	2	$B_c^2 = (\zeta + \alpha_{yy})\chi_{\perp}$	$B_s^2 = (\zeta + \alpha_{xx})\chi_{\perp}$	$B_t^2 = -B_t^1$
	4			

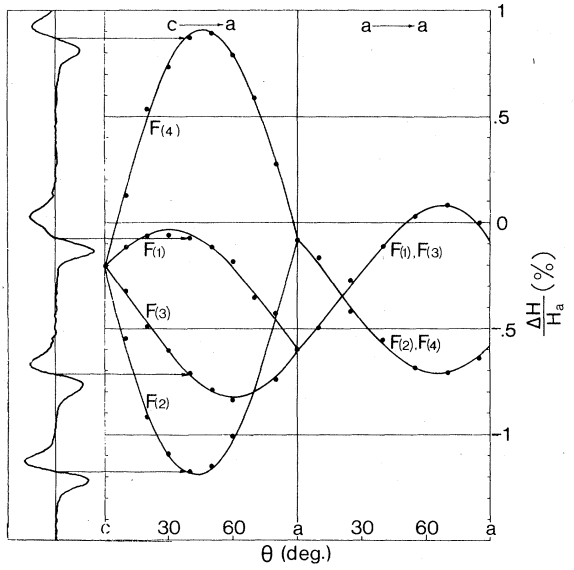

FIG. 2. Fluorine NMR rotation spectra for $LiDyF_4$. The dots are the measured points and the solid lines are the best fit. The origin of the individual lines is indicated by F(1),..., F(4) which correspond to the lettering in Fig. 1. The inset shows an actual recording for H in the c-a plane, 40 deg from the c axes. [Note the extra line near to the F(1) line due to fluorine in the lacquer on the coil wire.]

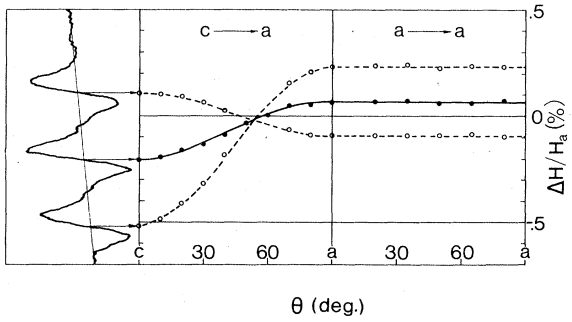

FIG. 3. Lithium NMR rotation spectra for $LiDyF_4$. The dots are the measured points, and the solid and broken lines are, respectively, the center transition ($\frac{1}{2} \longleftrightarrow -\frac{1}{2}$) and the satellite transitions ($\pm\frac{3}{2} \longleftrightarrow \pm\frac{1}{2}$). The satellites are due to the crystal-field interactions, which are not discussed in this paper. (All the spectra in the $a \rightarrow a$ rotation should be identical and they therefore give an impression of the experimental scatter.) The inset shows the actual recording for $\vec{H} \parallel \vec{I}_2$.

TABLE III. Fourier components of the relative magnetic field shifts at the Li and F site in %. Accuracy ±0.02%. Data extracted from the NMR rotation spectra. The underlined numbers are mean values.

		F						Li		
%		A_c	A_s	A_t	B_c	B_s	B_t	A_c	A_s	A_t
	1	−0.302	−0.551	−1.556	−0.481	−0.092	−0.441	−0.195	0.060	0.004
	3	−0.290	−0.516	1.630						
$LiTbF_4$			−0.534							
	2	−0.267	−0.083	−0.898	−0.111	−0.503	0.402			
	4	−0.304	−0.039	0.810						
		−0.291	−0.061							
	1	−0.197	−0.621	−0.713	−0.606	−0.051	−0.607	−0.203	0.070	0.027
	3	−0.218	−0.508	0.631						
$LiDyF_4$			−0.601							
	2	−0.212	−0.075	−2.097	−0.059	−0.622	0.506			
	4	−0.202	−0.083	2.101						
		−0.207	−0.079							
	1	−0.168	−0.627	−0.713	−0.693	−0.017	−0.541	−0.204	0.085	−0.015
	3	−0.184	−0.637	0.670						
$LiHoF_4$			−0.632							
	2	−0.194	−0.004	−2.256	−0.006	−0.677	0.564			
	4	−0.160	−0.050	2.207						
		−0.177	−0.027							
	1	−0.141	−0.622	−1.649	−0.591	−0.003	−0.556	−0.160	0.053	0.009
	3	−0.117	−0.650	1.619						
$LiErF_4$			−0.636							
	2	−0.125	−0.006	−0.905	−0.010	−0.588	0.567			
	4	−0.138	−0.017	0.853						
		−0.130	−0.012							

mergings for H_a in special directions, agrees with the theoretical expressions of Table II.

The ^{7}Li is a spin-$\frac{3}{2}$ nucleus, and therefore the resonance is split in three lines by the quadrupole effect. The information derived from this splitting has been explained elsewhere (Hansen *et al.*[1,2]). Because the quadrupole interaction is small compared to the Zeeman interaction, the paramagnetic shift is determined by the position of the center line or of the center of gravity of the satellite lines with sufficient accuracy.

IV. RESULTS

The series of spectra corresponding to the various rotations have been Fourier analyzed, and the components of other than zeroth and second order found negligible. The nonzero components are collected in Table III according to the notation introduced in (8) and Table II.

To extract the mean field tensors the room-temperature susceptibility tensors are needed. They are given by Hansen *et al.*[1,2] and reproduced in Table I.

The experimentally best determined mean-field tensors, which take into account all measured Fourier components, are given in Table IV for the fluorine site No. 1 and in Table V for the lithium site.

The dipole contribution $\overleftrightarrow{\delta}$ to $\overleftrightarrow{\alpha}$ at the lithium can be calculated using the cell dimensions given by Keller and Schmutz[16] (reproduced in Table I). The calculation of $\overleftrightarrow{\delta}$ at the fluorines in addition requires knowledge of the position of a fluorine in the unit cell. For $LiTbF_4$ this has been determined most accurate by neutron diffraction (Als-Nielsen *et al.*[27]), who found (0.220, 0.162, 0.331). It is assumed that the relative fluorine positions are the same in the other $LiRF_4$. With this assumption the $\overleftrightarrow{\delta}$ components of Tables VI and VII have been calculated, by lattice summation over spherical shells. (Convergence to better than 1% is achieved summing in a sphere with radius 40 Å). Finally subtracting $\overleftrightarrow{\delta}$ from $\overleftrightarrow{\alpha}$ the ITH ζ and ATH $\overleftrightarrow{\epsilon}$ shown in Tables VI and VII are obtained. The assignment of the four measured $\overleftrightarrow{\alpha}_F^j$ to the calculated $\overleftrightarrow{\delta}_F$ for fluorine Nos. 1, 2, 3, and 4 has been done such that $\overleftrightarrow{\epsilon}_F^j$ becomes as small as possible.

The accuracy of the results will now be considered: Because the Fourier components of the F spectra contain much redundancy, the standard deviation of $\overleftrightarrow{\alpha}_F$ can be calculated and gives ±1 g/cm^3. If the F positions are estimated to be known ±1% of the average lattice constant, the calculated $\overleftrightarrow{\delta}_F$ have an accuracy of ±2 g/cm^3. This means that ζ_F and $\overleftrightarrow{\epsilon}_F$ can be determined to within

TABLE IV. Expressions for $\overleftrightarrow{\alpha}_F^1$ components and ζ_F, which takes into account all measured Fourier components of the rotation spectra. The values shown (in g/cm^3) are calculated from these expressions.

	$a\rightarrow a$ and $c\rightarrow a$ scan $LiDyF_4$ and $LiHoF_4$	$a\rightarrow a$ and $c\rightarrow b$ scan $LiTbF_4$ and $LiErF_4$	$LiTbF_4$	$LiDyF_4$	$LiHoF_4$	$LiErF_4$
α_{xx}	$(4A_s^1-2A_s^2+2B_c^1-B_c^2-B_s^1+2B_s^2)/12\chi_\perp-A_c/3\chi_{\parallel}$	$[2(A_s^1+A_s^2)+3(B_c^1-B_c^2-B_s^1+B_s^2)]/12\chi_\perp-A_c/3\chi_{\parallel}$	−17.00	−13.92	−22.55	−22.38
α_{yy}	$(-2A_s^1+4A_s^2-B_c^1+2B_c^2+2B_s^1-B_s^2)/12\chi_\perp-A_c/3\chi_{\parallel}$	$[2(A_s^1+A_s^2)-3(B_c^1-B_c^2-B_s^1+B_s^2)]/12\chi_\perp-A_c/3\chi_{\parallel}$	11.70	11.34	15.05	15.00
α_{xy}	$(B_t^1-B_t^2)/4\chi_\perp$	$+(A_s^1-A_s^2+B_t^1-B_t^2)/6\chi_\perp$	−16.87	−13.00	−14.77	−18.66
α_{xz}	$(A_t^1-A_t^3)/2(\chi_{\parallel}+\chi_\perp)$	$+(A_t^1-A_t^2-A_t^3+A_t^4)/2\sqrt{2}\,(\chi_{\parallel}+\chi_\perp)$	−15.15	−17.32	−18.49	−18.41
α_{yz}	$(A_t^2-A_t^4)/2(\chi_{\parallel}+\chi_\perp)$	$+(A_t^1+A_t^2-A_t^3-A_t^4)/2\sqrt{2}\,(\chi_{\parallel}+\chi_\perp)$	−50.15	−54.10	−59.66	−61.27
ζ		$[2(A_s^1+A_s^2)+B_c^1+B_c^2+B_s^1+B_s^2]/12\chi_\perp+A_c/3\chi_{\parallel}$	−19.20	−14.69	−16.18	−16.52

TABLE V. α_{xx} and ζ at the Li site in g/cm^3.

		$LiTbF_4$	$LiDyF_4$	$LiHoF_4$	$LiErF_4$	Accuracy
α_{xx}	$\frac{1}{3}(A_S/\chi_\perp - A_c/\chi_\parallel)$	4.58	4.98	5.00	5.14	±1
ζ	$\frac{1}{3}(2A_S/\chi_\perp + A_c/\chi_\parallel)$	−0.17	−1.71	−0.01	−1.71	±1

±1 g/cm^3 and ±3 g/cm^3, respectively.

The accuracy of $\vec{\vec{\alpha}}_{Li}$ is judged also to be ±1 g/cm^3. For Li, occupying a special site in the lattice, the uncertainty in $\vec{\vec{\delta}}$ is negligible and therefore ζ_{Li} and $\vec{\vec{\epsilon}}_{Li}$ are probably both determined to within ±1 g/cm^3.

It is noticed (Table VI) that at the fluorine site there is a negative ITH whereas the ATH is almost negligible taking into account the accuracy of the measurements. Likewise (Table VII) at the lithium site there seems to be a (numerically much smaller) negative ITH, and no measurable ATH. (The *difference* between the Li ITH for the various compounds is probably of the order of the accuracy and thus insignificant. It is only claimed that there is a common negative Li ITH around −0.9 ±1.0 g/cm^3).

It is seen from Fig. 1 that the fluorines are nearest neighbors to the rare earths, placed ~2.4 Å away, and the lithiums are next nearest neighbors to the rare earths, ~3.8 Å removed. It is therefore understandable that the ITH is much stronger at the fluorine site, than at the lithium site.

V. DISCUSSION OF ^{19}F RESULTS

A frequently used assumption[22,28,29] has been to write the interaction between the resonating nucleus and the R ions in the form

$$\mathcal{H} = \vec{I}_n \cdot \vec{\vec{A}}_n \cdot \vec{S}, \tag{9}$$

where $\vec{I}_n$ is the dimensionless angular momentum operator for the ^{19}F or ^{7}Li nuclei, $\vec{S}$ the electronic spin operator for the rare-earth ions, and $\vec{\vec{A}}_n$ is a tensor containing both the isotropic and anisotropic transferred hyperfine interaction. Assuming that ζ_n has only contributions from nearest-neighbor R's to the resonating nuclei, one can determine the strength of the isotropic interaction between a nuclear spin and a single R ion:

$$A_n^{iso} = \frac{1}{N_n}\frac{\zeta_n}{\kappa}\frac{g_J}{g_J - 1}\mu_B\gamma_n. \tag{10}$$

Here N_n is the number of nearest-neighbor R to the interacting nucleus ($N_F = 2$, $N_{Li} = 8$), g_J the Landé factor for the rare-earth ion (see Table I), μ_B the Bohr magneton, and $\gamma_F = 4.006$ kHz/G and $\gamma_{Li} = 1.655$ kHz/G are the nuclear gyromagnetic ratios. A_n^{iso} in turn is often interpreted in terms of the Fermi contact mechanism operating at the ligand nucleus. From (10) it is clear that due to the factor $(g_J - 1)$ the NMR shift should differ in sign for the light and heavy rare-earth ions, if A^{iso} is of constant sign. Some of the first measurements of the paramagnetic shifts for rare earth ions were made by Lewis *et al.*[28] on R ions dissolved in water, and for the resonances of ^{17}O this sign shift was found. The sign at A^{iso} was negative for all rare-earth ions in agreement with the polarization mechanism proposed by Freeman and Watson.[30] However, as discussed by Kurland and McGarvey[31] an implicit assumption in (9) is that the hyperfine interaction A^{iso} is the same for all states in the lowest crystal-field split multi-

TABLE VI. Tensor values for the fluorine site. (1) The dipole field tensor $\vec{\vec{\delta}}$ components in g/cm^3 calculated by lattice summation in a sphere with radius 40 Å. Accuracy ±1 g/cm^3. (2) The ATH $\vec{\vec{\epsilon}}$ components in g/cm^3 obtained by subtracting $\vec{\vec{\delta}}$ from the experimental $\vec{\vec{\alpha}}$. Accuracy ±3 g/cm^3. (3) The ITH ζ in g/cm^3. Accuracy ±2 g/cm^3.

		$LiTbF_4$	$LiDyF_4$	$LiHoF_4$	$LiErF_4$
(1) $\vec{\vec{\delta}}$	δ_{xx}	−18.05	−18.75	−19.03	−19.32
	δ_{yy}	11.99	12.42	12.64	12.87
	δ_{xy}	−16.76	−17.34	−17.45	−17.68
	δ_{xz}	−16.06	−16.90	−17.74	−18.20
	δ_{yz}	−54.34	−55.94	−57.26	−58.35
(2) $\vec{\vec{\epsilon}}$	ϵ_{xx}	1.05	4.83	−3.52	−3.06
	ϵ_{yy}	−0.29	−1.08	2.41	2.13
	ϵ_{xy}	−0.11	4.34	2.68	−0.98
	ϵ_{xz}	−0.91	−0.42	−0.75	−0.21
	ϵ_{yz}	4.19	1.84	−2.40	−2.92
(3) ζ		−19.20	−14.69	−16.18	−16.52

TABLE VII. Tensor values for Li. (1) The dipole field tensor $\overleftrightarrow{\delta}$ components in g/cm^3 calculated by lattice summation in a sphere with radius 40 Å (convergence better than 1%). (2) The ATH components (negligible small) in g/cm^3 obtained by subtracting $\overleftrightarrow{\delta}$ from the experimental $\overleftrightarrow{\alpha}$. (3) The average ITH ζ in g/cm^3.

	$LiTbF_4$	$LiDyF_4$	$LiHoF_4$	$LiErF_4$	Remarks	Accuracy
(1) $\delta_{xx}=\delta_{yy}$	4.87	4.98	5.05	5.06		±1
(2) $\epsilon_{xx}=\epsilon_{yy}$	−0.29	0.00	−0.05	0.08	~0	±1
(3) ζ		~−0.9			Only average value	±1

plet of the rare-earth ions. For the covalent model analyzed by Axe and Burns,[32] Baker,[33] and McGarvey[34,35] this assumption is not valid. The form (9) has been used in the interpretation of low-temperature ESR and electron-nuclear double-resonance measurements, where only the ground doublet is populated. For the CdF_2-YbF_3 system Mustafa *et al.*[24] found a sign difference between the isotropic hyperfine constant derived at high and low temperature, indicating that (9) is oversimplified. What has been found until now is, that, at low temperatures, the covalent model is describing the ^{19}F shift coming from Tm^{2+} and Yb^{3+} reasonably well, while the sign of A^{iso} for Gd^{3+} and Eu^{2+} indicates that for these ions the polarization mechanism is dominating.

In view of the situation just described we have in this paper chosen to reduce the raw experimental data in terms of the phenomenological, temperature-dependent parameters ζ_n and $\overleftrightarrow{\epsilon}_n$ defined through Eq. (2). It should be noted that at 295 K we are at or above the high-temperature limit of these systems with respect to crystal-field splittings, and that in this region ζ and $\overleftrightarrow{\epsilon}$ will be approximately temperature independent. As the results have shown the anisotropic part $\overleftrightarrow{\epsilon}$ to be small compared to ζ, whereas the anisotropy in $\overleftrightarrow{\chi}$ is in some cases rather big, this method of representation seems convenient for uniaxial systems.

Clearly a systematic study of the paramagnetic shift as a function both of temperature — in a wide range — as well as of the rare earth species for a fixed compound is warranted, in order to clarify the different mechanisms, which give rise to the paramagnetic shift in these systems. We plan to make such a study; preliminary measurements indicate that broadening of the NMR lines with decreasing temperature may present a difficulty. This broadening is attributed to a slowing down of the relaxation rate in the rare-earth spin system, starting at rather high temperatures because of the absence of strong exchange in these systems. However, with the approximate knowledge of crystal-field effects for all the heavy rare earth in $LiRF_4$, several model examples can be hoped for.

VI. SUMMARY

The transferred hyperfine interaction in the simple crystals $LiRF_4$ (R = Tb, Dy, Ho, and Er) with the Li and F nuclei have been measured. The anisotropic part of this interaction is for both nuclei negligible compared to the isotropic part. For F the isotropic interaction is of the same order as the F-R dipole interaction, whereas for Li it is five times smaller than the Li-R dipole interaction.

Our results together with the existing data suggest that in general several mechanisms may be needed to explain the transferred hyperfine interaction for the rare earth, and that measurements as a function of temperature could partially resolve the problem.

ACKNOWLEDGMENTS

The authors are grateful to Professor V. Frank for his continued interest. It is a pleasure to thank Professor B. R. McGarvey for preprints of recent work and for many valuable suggestions.

*Work partly supported by the Danish Natural Science Research Council, Grant No. 511-3575.

[1]P. E. Hansen, T. Johansson, and R. Nevald, Phys. Rev. B 12, 5315 (1975).
[2]R. Nevald and P. E. Hansen, Physica B 86, 4F3 (1977).
[3]J. M. Baker and J. P. Hurrell, Proc. Phys. Soc. Lond. 82, 742 (1963).
[4]R. G. Bessent and W. Hayes, Proc. R. Soc. A 285, 430 (1965).
[5]U. Ranon and J. S. Hyde, Phys. Rev. 141, 259 (1966).
[6]J. M. Baker, E. R. Davies, and J. P. Hurrell, Proc. R. Soc. A 308, 403 (1968).
[7]D. Kiro and W. Low, Phys. Rev. Lett. 20, 1010 (1968).
[8]R. H. Borcherts, T. Cole, and T. Horn, J. Chem. Phys.

49, 4880 (1968).
[9]H. Bill, Phys. Lett. A 29, 593 (1969).
[10]R. Valentin, Phys. Lett. A 30, 344 (1969).
[11]K. Baberschke, Phys. Lett. A 34, 41 (1971).
[12]Te-Tse Chang, M. I. Cohen, and W. R. Hosler, J. Chem. Phys. 54, 4278 (1971).
[13]T. C. Ensign, J. Chem. Phys. 54, 5188 (1971).
[14]J. M. Baker and W. B. J. Blake, J. Phys. C 6, 3501 (1973).
[15]E. Secemski and W. Low, Phys. Rev. B 9, 4954 (1974).
[16]S. Lee, A. J. Bevolo, and Chi-Chung Yang, J. Chem. Phys. 60, 1628 (1974).
[17]C. H. Anderson, P. Call, J. Stott, and W. Hayes, Phys. Rev. B 11, 3305 (1975).
[18]J. M. Baker and T. Christidis, J. Phys. C 8, L334 (1975).
[19]Chi-Chung Yang, S. Lee, and A. J. Bevolo, Phys. Rev. B 13, 2762 (1976).
[20]J. P. Wolfe and R. S. Markiewicz, Phys. Rev. Lett. 30, 1105 (1973).
[21]W. Saraswati and R. Vijayaraghavan, J. Phys. Chem. Solids 28, 2111 (1967).
[22]S. L. Carr and W. G. Moulton, J. Magn. Reson. 4, 400 (1971).
[23]E. Banks, M. Greenblatt, and B. R. McGarvey, J. Chem. Phys. 58, 4787 (1973).
[24]M. R. Mustafa, W. E. Jones, B. R. McGarvey, M. Greenblatt, and E. Banks, J. Chem. Phys. 62, 2700 (1975).
[25]I. Laursen and L. M. Holmes, J. Phys. C 7, 3765 (1974).
[26]C. Keller and H. Schmutz, J. Inorg. Nucl. Chem. 27, 900 (1965).
[27]J. Als-Nielsen, L. M. Holmes, F. Krebs Larsen, and H. J. Guggenheim, Phys. Rev. B 12, 191 (1975).
[28]W. B. Lewis, J. A. Jackson, J. F. Lemons, and H. Taube, J. Chem. Phys. 36, 694 (1962).
[29]F. Friedman and J. Grunzweig-Genossar, Phys. Rev. B 4, 180 (1971).
[30]R. E. Watson and A. J. Freeman, Phys. Rev. 156, 251 (1967).
[31]R. J. Kurland and B. R. McGarvey, J. Magn. Reson. 2, 286 (1970).
[32]J. D. Axe and G. Burns, Phys. Rev. 152, 331 (1966).
[33]J. M. Baker, J. Phys. C 1, 1670 (1968).
[34]B. R. McGarvey, J. Chem. Phys. 65, 955 (1976).
[35]B. R. McGarvey, J. Chem. Phys. 65, 962 (1976).